Modeling The Interaction Between a Rocket Plume, Scoured Regolith, and a Plume Deflection Fence

A. B. Morris[1], D. B. Goldstein[1], P. L. Varghese[1], and L. M. Trafton[2]

[1]ASE-EM Dept., [2]Astronomy Dept., The University of Texas at Austin, 1 University Station, C0600, Austin, TX 78712; Ph (512) 471-7205; email: morria2@gmail.com

ABSTRACT

As a lunar lander approaches the surface, the impinging exhaust gases entrain regolith into a high velocity spray. This two-phase spray can be damaging to nearby structures, such as a lunar outpost. One way of mitigating this damage is to use a berm or fence to shield nearby structures from the dust spray. In this work, we use a coupled continuum – DSMC (direct simulation Monte Carlo) solver to simulate the gas and dust flow fields. A continuum solver, DPLR, is used to model the internal nozzle flow from the nozzle throat out to the continuum regions of the under-expanded exhaust in the near vicinity of the engine. As the rocket exhaust expands further towards vacuum, continuum assumptions break down and kinetic equations are used. Additionally, a dust – gas collision model that conserves momentum and energy transfer between the gas and dust grains has been implemented into the kinetic solver. The distance of the deflection fence from the landing pad is studied parametrically and the corresponding gas and dust flow fields are analyzed. Additionally, the sensitivity of the model to the dust – fence coefficient of restitution is studied when the fence is located 15 m off axis.

INTRODUCTION

As a lunar lander approaches the surface, the rocket engine exhaust plume strikes the ground causing dust and larger debris to be entrained into the flow field. During the Apollo moon landings, the dust erosion posed several operational hazards, including obscuration of the pilot's vision, degradation of mechanical components, damage to space suit seals, and clogging of thermal rejection systems (Gaier, 2005). The Apollo 12 lunar module, LM, landed 163 m away from the Surveyor III spacecraft, and it was found that the Surveyor surfaces that were facing the LM were pitted and coated in dust (Immer, 2011). Lunar dust poses difficulties atypical of terrestrial soils because a major component of it consists of a fine powder that is exceptionally rough at the microscopic scale. This property arises from constant micrometeorite bombardment and negligible atmospheric weathering (Heiken, 1991). An unfortunate consequence of the jagged and irregular shape of lunar regolith grains is that they can adhere to nearly any surface they contact. During landing, eroded dust sprays that are unimpeded by a background atmosphere travel nearly parallel to the surface with velocities that are O(1000 m/s). Erosion angles have been inferred by photogrammetry of the landing videos (Immer, 2011) and also modeled by (Lane, 2008 and Morris, 2010). One method for protecting nearby structures is to use a fence or berm to shield sensitive structures from the dust spray. The flow about such

flow obstacles may, however, be transitional between the continuum and free molecular regimes; thus the DSMC method is used to capture non-equilibrium effects in our work described below.

METHOD

When near the lunar surface, the exhaust gases in the vicinity of the rocket engine are highly collisional and can be simulated using continuum assumptions. However, as the flow expands towards vacuum, continuum assumptions break down and a kinetic model, e.–g. DSMC (Bird, 1994), must be used. Although DSMC is valid for both the continuum and non-equilibrium regimes, the high collision rates and small mean free paths in the near field make DSMC computationally expensive and impractical. We use an alternate hybrid approach where the near field is solved via the Navier Stokes solver DPLR (Wright, 1998), and the far field is solved using DSMC. This coupled approach has been previously used for modeling plume impingement effects, (Lumpkin 2007).

Continuum Regime.

The continuum solver DPLR is used to solve for the flow field inside the expanding section of the engine bell as well as the near field flow where the engine exhaust is strongly under-expanded. In the current work, we chose to model a descent engine similar to the Lunar Module descent engine because this allows us to compare to certain data from the Apollo landings. The LM descent engine was a hypergolic engine that burned Aerozine-50 and nitrogen tetroxide. In reality the exhaust gases are comprised of many different species, but only the most prevalent species, H_2O (Simoneit, 1969), is presently included in our model. Near touchdown, the thrust of the descent engine was approximately 3,000 lbs and the ISP was 305 s (Hammock 1973). The area ratio of the expander was 47.5 and the diameter at the nozzle exit plane was 1.32 m. Given these specifications, the mean exit plane density, velocity, and temperature are expected to be about 1.1×10^{-3} kg/m^3, 2992 m/s, and 525 K, respectively. Isentropic flow relations are used to determine the corresponding throat conditions that are then used as our boundary condition. DPLR has the ability to simulate many different types of physics, but in our subsequent calculations we assume the flow is axi-symmetric, steady, laminar, in rotational and vibrational equilibrium, and not radiating or chemically reacting. Figure 1 shows contours of number density and the exit plane properties of the nozzle obtained with DPLR. The actual thrust of the modeled engine is 2960 lbs and the mean exit plane density, velocity, and temperature are 1.18×10^{-3} kg/m^3, 2860 m/s, and 577 K. Although the continuum solver accurately models the near field, it incorrectly predicts a barrel shock further out because we must apply a boundary condition of a small atmospheric pressure. In reality this would not occur because the exhaust gases expand to vacuum. Hence, we choose our hybrid interface within the shock so that the background atmosphere is irrelevant.

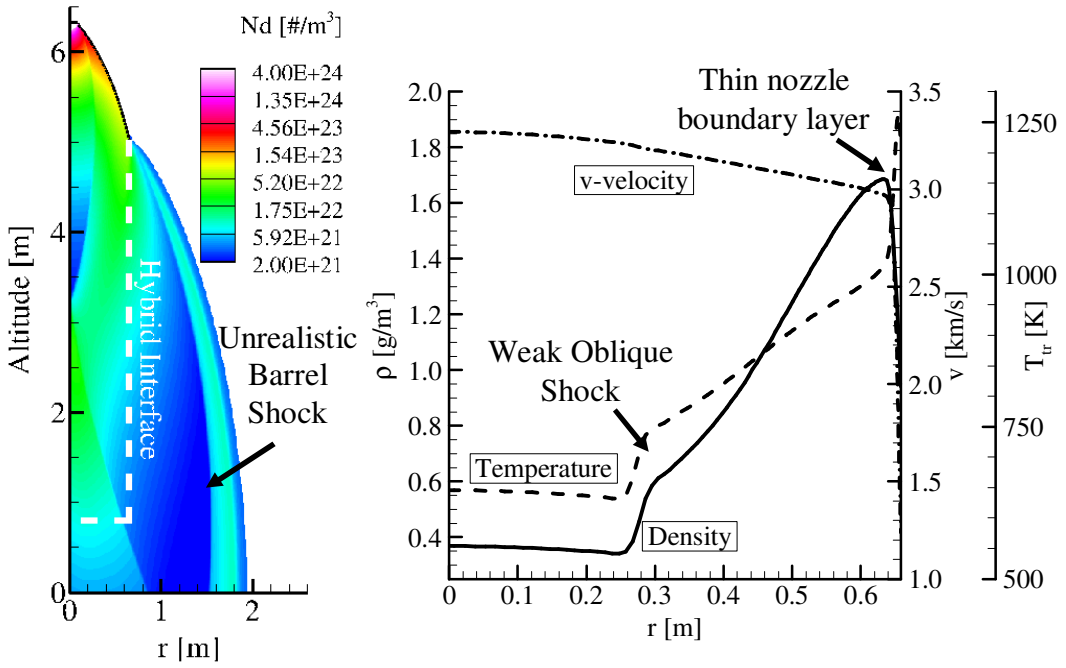

Figure 1. (left) Number density contours from the continuum solver, DPLR. The interface where the continuum solver couples to DSMC is indicated by the dashed line. (right) Macroscopic properties at the exit plane of the nozzle.

Rarefied Regime.

A common method for solving for transitional-to-rarefied flows is to use the direct simulation Monte Carlo method. DSMC is a particle method that simulates a gas flow on the microscopic level. Basic DSMC uses simulated molecules that represent many more real gas molecules and these simulated molecules travel ballistically and can occasionally collide with each other. Collisions are treated as brief, instantaneous events which change the molecular velocity. Throughout the years, more sophisticated physical models have been applied to DSMC, and the relevant physical models in our work include both rotational and vibrational energies, variable hard sphere cross sections, gas – particle interactions, and a hybridization scheme that allows for greater efficiency by coupling the DSMC to DPLR solutions. The hybridization is a loosely-coupled approach (Roveda, 1998), where the continuum solution feeds into the DSMC regime, but the DSMC solution does not feedback to the continuum solver. The continuum flow is first solved and an interface is drawn, Figure 1, where the flow is both continuum and the flow velocity normal to the interface is supersonic. Volume reservoir cells are created along this interface and are populated with molecules from a Maxwellian distribution based on the corresponding macroscopic properties from the continuum solution. These molecules then behave as regular DSMC molecules and can convect into the computational domain. Our DSMC simulations use an adaptive linear cell stretching method (Moore, 2011) to achieve mean free path resolution near the fence. Simulations were performed on the Texas Advanced Computing Cluster using 36 processors, 1,008,000 collision cells, and a timestep of 2 μs.

Dust – Gas Interactions.

Within the context of DSMC, dust particles are simply treated as a special species whose size and mass are significantly larger than typical gas molecules. Further, each dust particle has a temperature which represents the energy stored within the lattice of the grain while gas molecules, analogously, have internal energy that can be stored in rotational or vibrational modes. Previous work has indicated that the mass fraction of dust within the entraining gas flow is significant, and consequently we need a fully coupled gas – particle model that allows for both the gas and dust to affect one another; as momentum and energy are transferred to the dust grains, momentum and energy are also conservatively removed from the gas. A fully coupled gas – particle model (Burt, 2004 and Gallis, 2001) is used in this work. In these models, gas molecules collide with dust grains, and can be reflected either diffusely or specularly from the dust grain. Because of the highly irregular geometry of our regolith grains, all gas molecules are assumed to reflect diffusely with a relative speed characteristic of the grain temperature. Analytic expressions for the drag and heat transfer to the dust grains are obtained by integrating over all possible impact parameters (Gallis, 2001). It is important to note that these models assume the local flow about each grain is free-molecular, i.e. the gas mean free path is large relative to the grain diameter, and structures such as boundary layers and shocklets around the grains are neglected. Although one could use a more sophisticated drag model that accounts for compressibility and finite Re effects (Loth, 2008), it would be difficult to fully couple such a model because the gas flow is not resolved on length scales associated with boundary layers over individual grains. To quantify the consequence of our free molecular assumption, grain based Kn numbers are calculated for typical landing conditions, and the corresponding drag coefficients predicted by Loth's equations are then compared to free molecular models, Figure 2.

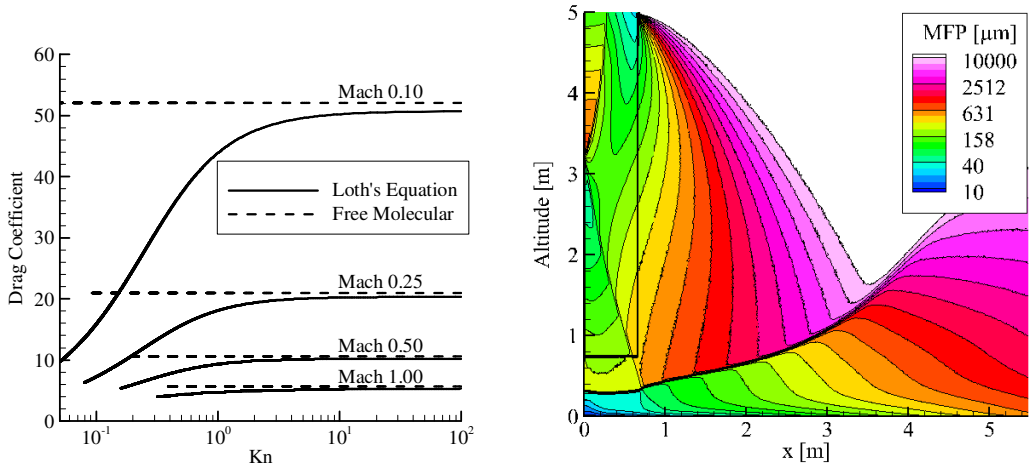

Figure 2. (left) Drag Coefficient versus Kn number for Loth's equation (solid) and free molecular (dashed) models for subsonic relative (gas – grain) Mach numbers. (right) Gas mean free path contours in the near field. Typical grain sizes are between 1 μm and 100 μm.

Near the stagnation point, the gas mean free path is approximately 25 microns, thus the Kn numbers for the smallest grains are expected to be of order unity near the stagnation point. Consequently, free molecular drag coefficients may be ~5% larger than more sophisticated models such as Loth's would suggest, but this only occurs for the largest grains and these errors decrease rapidly as the flow expands to a couple of meters off axis where peak erosion is expected.

Erosion Model.

Several different mechanisms for erosion have been identified in Metzger (2011) where it is suggested that viscous erosion is the dominant mechanism for lunar landings. Viscous erosion occurs when the shear stress on the surface exceeds the cohesive strength of the soil, causing loose grains to slide or roll along the surface. These grains can impact neighboring grains which cause them to "hop" and subsequently become entrained by the gas flow. Scaling relationships for viscous erosion rates have been identified (Metzger, 2010), and it was found that the erosion rate scales with the densimetric Froude number.

$$\Phi_e = C \frac{\rho_g U_g^2}{2 g \rho_p D_p} \qquad (1)$$

The left hand side of equation 1 represents the particle mass flux, $\rho_g U_g^2/2$ is the dynamic pressure of the free stream gas outside of the viscous boundary layer, ρ_p is the density of the dust grain, g is the acceleration of gravity, D_p is the diameter of the dust grain, and C is a constant. The dynamic pressure is evaluated at a distance slightly above the boundary layer because the surface roughness scales are assumed to be large relative to the boundary layer scale. The constant C is selected such that the erosion rate closely matches net erosion rates typical of the Apollo landings (Immer, 2011). In our simulations, the scaling coefficient is set to 2.5×10^{-9} kg/m^2-s. A typical erosion profile when the rocket engine hovers at an altitude of 5 m is shown in Fig. 3. At this altitude, the peak erosion occurs relatively close to the axis of symmetry, r~1 m, and is unaffected by the presence of a lunar fence for most cases.

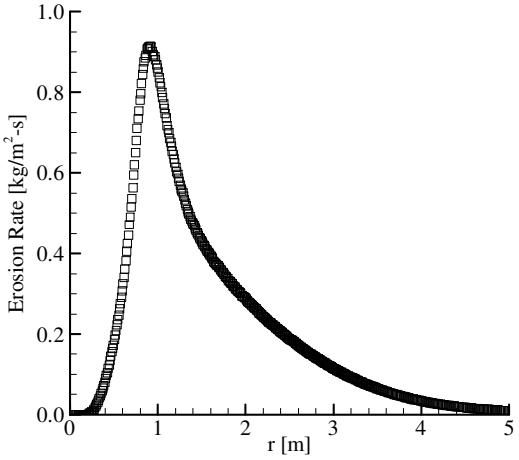

Figure 3. Erosion profile for axisymmetric hover 5 m above the lunar surface.

Dust – Surface Interactions.

When dust grains strike the lunar surface, it is possible to have secondary erosion by saltation. This process is neglected in the current work and dust grains that strike the lunar surface are assumed to stick. Gas molecules, however, reflect diffusely with an assumed surface temperature of 500 K. However, when dust grains strike obstacles such as a lunar fence, they have a large normal velocity and are expected to recoil somewhat. This is simply modeled by assuming a tangentially specular reflection with an assumed coefficient of restitution for the normal velocity component. The coefficient of restitution, α_{cor}, can have a large impact on the resulting flow fields and it is assumed to depend strongly on the fence and grain material properties. Gas molecules are assumed to diffusely reflect from the fence.

RESULTS

Fence Effectiveness.

In the following simulations, 1 μm grains impact fences placed 10 m, 15 m and 20 m from the landing pad and the wall normal coefficient of restitution was set to 0.5. Simulations where the fence is closer to the symmetry axis can show weak unsteady behavior in the shedding of dust over the top of the fence. This unsteadiness is not yet fully understood, but it diminishes as the fence is moved further from the landing pad. Regardless, in the current work we present time averaged data when the solution reaches an apparent steady state. In Fig. 4, the fence is placed 10 m from the jet axis and horizontal velocity contours of the dust grains are shown. At this location, the gas is sufficiently dense that the dust grains rebound only 2 m upstream of the fence before being turned by the gas flow. Incident grains that strike the bottom of the fence near the lunar surface are typically moving with a lower velocity. When these low momentum grains clear the lunar fence, they are more easily deflected downwards by the gas flow and can impact the lunar surface again slightly downstream of the fence. Although the fence does not shield leeward structures completely, it vastly reduces the downstream grain velocities and deflects the bulk of the dust momentum upwards.

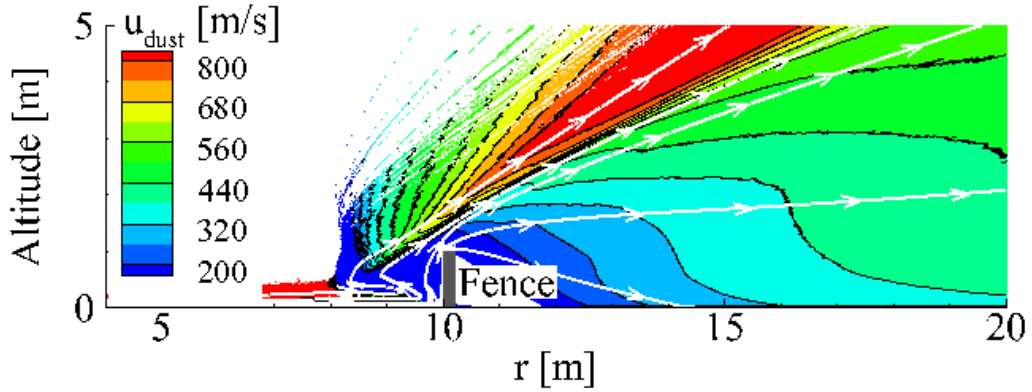

Figure 4. Horizontal velocity contours for the dust grains interacting with a deflection fence placed 10 m from the jet axis. Note dust "streamlines" are an equilibrium property and may be misleading upstream of the fence where dust sprays are passing through eachother.

As the fence is progressively moved outwards, Figure 5, the dust grains tend to bounce further off the fence and the grain velocities downstream of the fence decrease. The larger bounces occur because the incident dust grain velocities are typically higher and the coupling between the dust and gas decrease as the gas expands to lower densities. These results also suggest that when the fence is placed 20 m from the jet axis, structures less than 1 m tall are completely shielded from the dust spray.

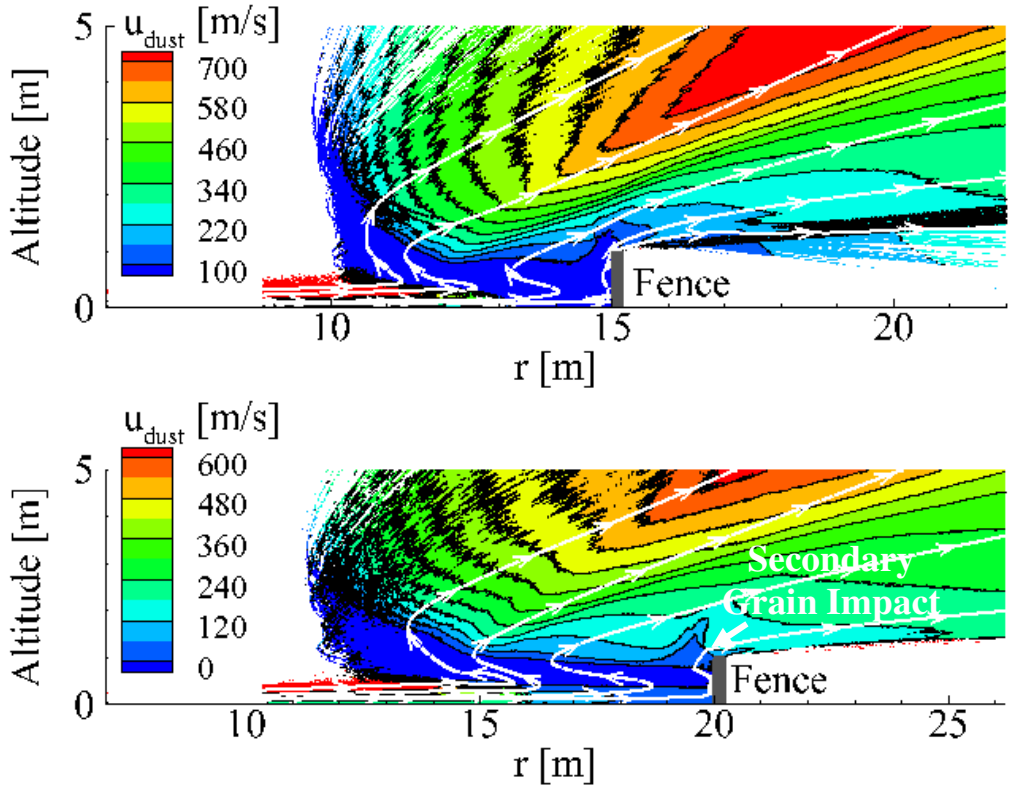

Figure 5. Horizontal velocity contours for the dust grains interacting with a deflection fence (α_{cor} = 0.5) placed 15 m (top) and 20 m (bottom) from the jet axis.

It should be noted that the velocity is computed by averaging the velocities of all dust grains in a given cell. This can be misleading because near the fence half of the dust grains are moving to the right with a high velocity while the other half are moving left. For specular reflection, the averaged velocity would thus be zero while the individual grains actually have very high velocities. This may also be misleading for the dust streamlines upstream of the fence.

Fence Coefficient of Restitution.

The dust – fence interaction can have a significant impact on the resulting flow fields and consequently the fence effectiveness. As previously stated, the gas molecules reflect diffusely from the fence and are not directly affected by an assumed coefficient of restitution for dust. In Figure 6, contours of number density for 1 micron dust grains that interact with a fence located 15 m from the jet axis are presented. To illustrate the coupled response of the gas flow field, line contours of gas number density are also drawn.

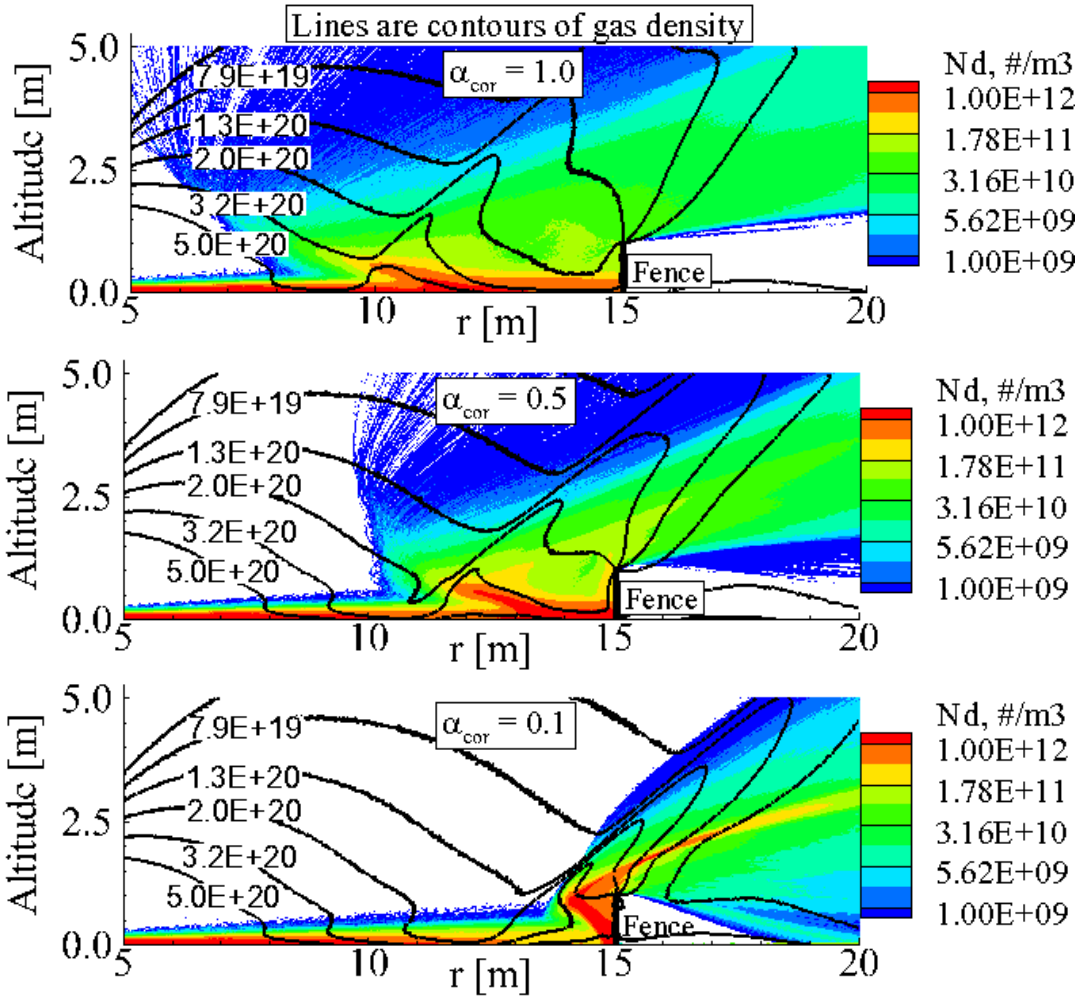

Figure 6. Contours of dust number density for wall normal coefficient of restitution values of 0.1, 0.5, and 1.0. The line contours are for the gas number density.

In all cases, the tangential coefficient of restitution is 1. For specular reflections (α_{cor}=1.0), the dust grains rebound approximately 8 m upstream of the fence before they are turned by the flow. As the coefficient of restitution is decreased to 0.5 and 0.1, the grains rebound by approximately 5 m and 1 m, respectively. When the free stream gas flow impacts the reflected dust spray, the gas is compressed because of the relatively high mass loading of dust; approximately 90% dust at the shock foot. The foot of the oblique shock is approximately 5 m upstream of the fence for specular dust reflections, and moves closer to the deflection fence as the coefficient of restitution decreases. Additionally, the dust grains that deflect over the fence have less momentum as the coefficient of restitution decreases and are more readily deflected downward by the expanding gas. These results suggest that the dust – fence interaction model can have a large impact on the grain motion, especially at distances further from the axis where the gas density is relatively low.

CONCLUSIONS

A model that fully couples particle motion to the gas kinetics has been implemented into our hybrid DSMC solver. This work has focused on the effects of modeling a 1 m tall fence at various distances from the landing pad. For 1 micron particles, the fence was effective in all cases at reducing the grain velocities downstream of the fence. For fence locations close to the jet axis, the dust grains are initially deflected over the fence but are then turned downward by the expanding gas. As the fence is moved outwards, the dust grains are not as deflected downward by the gas because at these locations the gas density has decreased and the dust motion is less coupled to the gas. In future work, a more effective fence orientation may be to angle the fence such that dust grains are deflected upwards while retaining their forward momentum. It was also found that the solutions are sensitive to the wall normal coefficient of restitution. For specular grain reflections, the dust grains have a large rebound velocities compared to reflections with lower coefficients of restitution. Consequently, when the specularly reflected grains pass over the fence they typically have more inertia and are less turned by gas. Grain – grain collisions are normally infrequent because the relative velocity between grains is small. However, when grains bounce off of the fence, the relative velocity can be quite large and grain – grain collisions may not be negligible. We expect such collisions to have a significant impact especially when the fence is placed close to the axis of symmetry where the dust number density is large. Future work will include grain – grain collisions as well as parametric studies of geometric parameters.

ACKNOWLEDGEMENTS

Support for this work was provided under the NASA LASER program. Simulations were performed at the Texas Advanced Computing Center.

REFERENCES

Bird, G. (1994). *Molecular Gas Dynamics and the Direct Simulation of Gas Flows*, Clarendon Press, Oxford.

Burt, J. M., et. al (2004). "Development of a Two-Way Coupled Model for Two-Phase Rarefied Flows", AIAA Paper 2004-1351.

Gaier, J. R. (2005). "The Effects of Lunar Dust on EVA Systems During the Apollo Mission", NASA/TM-2005-213610, NASA Glenn Research Center, Cleveland, OH.

Gallis, M. A., et. al. (2001). "An Approach For Simulating the Transport of Spherical Particles in a Rarefied Gas Flow Via the Direct Simulation Monte Carlo Method," *Phys. Fluids*, **13**, No 11., pp 3482-3494.

Hammock, W., et. al.(1973). "Apollo Experience Report – Descent Propulsion System", Nasa TN D-7143, Manned Spacecraft Center, Houston, TX.

Heiken, G., et. al., (1991). *Lunar Sourcebook: A User's Guide to the Moon*, Cambridge University Press, Cambridge.

Immer, C., et. al, (2011). “Apollo Video Photogrammetry Estimation of Plume Impingement Effects”, *Icarus*, **214**, pp 46-52.

Immer, C., et. al. (2011). “Apollo 12 Lunar Module Exhaust Plume Impingement on Lunar Surveyor III.” *Icarus*, **211**, pp 1089-1102.

Lane, J., et al.,(2008). “Lagrangian Trajectory Modeling of Lunar Dust Particles”, *in Proc. of Earth and Space* 2008, Long Beach, CA.

Loth, et. al., (2008). “Compressibility and Rarefaction Effects on Drag of a Spherical Particle,” *AIAA Journal*, **46**, pp 2219-2228.

Lumpkin, F., et al., (2007) "Plume Impingement to the Lunar Surface: A Challenging Problem for DSMC", presented at the Direct Simulation Monte Carlo, Theory, Methods, and Applications Conference, Santa Fe, NM..

Metzger, P. T., et. al., (2010). “Scaling of Erosion Rate in Subsonic Jet Experiments and Apollo Lunar Module Landings,” *in Proc. of Earth and Space 2010*, Honolulu, HI.

Metzger, P. T., et. al., (2011). “Phenomenology of Soil Erosion Due to Rocket Exhaust on the Moon and the Mauna Kea Lunar Test Site,” *J. Geophysical Research*, **116**, E06005, doi:10.1029/2010JE003745.

Moore, C. H. (2011). “Monte Carlo Simulation of the Jovian Plasma Torus Interaction with Io’s Atmosphere and the Resultant Aurora during Eclipse”. Ph.D dissertation, The University of Texas At Austin, pp 38 – 49.

Morris, A. B., Goldstein, D. B, Varghese, P. V., Trafton, L. M. (2010). “Plume Impingement on a Dusty Lunar Surface”, in *Proc. of the 27th Intl. Symp. On Rarefied Gas Dynamics*, Pacific Grove, CA, pp 1187-1192.

Roveda, R., et. al. (1998). “A Hybrid Euler/DSMC Approach to Unsteady Flows”, *In Proc of the 21st Rarefied Gas Dynamics Conference*, **2**, pp 117-224.

Simoneit, B. R., et. al.,(1969). "Apollo Lunar Module Engine Exhaust Products", *Science*, **166**, No. 3906, pp. 733-738.

Wright, M. G., Candler, G. V., Bose, D. (1998). *AIAA Journal*, **36**, No. 9, pp 1603-1609.